

MIT Open Access Articles

*Particle dispersion by random waves
in the rotating Boussinesq system*

The MIT Faculty has made this article openly available. **Please share**
how this access benefits you. Your story matters.

Citation: Holmes-Cerfon, Miranda, Oliver Bühler, and Raffaele Ferrari. "Particle Dispersion by Random Waves in the Rotating Boussinesq System." *Journal of Fluid Mechanics* 670 (2011): 150–175. © Cambridge University Press 2011

As Published: <http://dx.doi.org/10.1017/s0022112010005240>

Publisher: Cambridge University Press

Persistent URL: <http://hdl.handle.net/1721.1/73682>

Version: Final published version: final published article, as it appeared in a journal, conference proceedings, or other formally published context

Terms of Use: Article is made available in accordance with the publisher's policy and may be subject to US copyright law. Please refer to the publisher's site for terms of use.



Journal of Fluid Mechanics

<http://journals.cambridge.org/FLM>

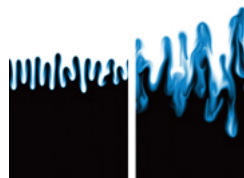
Additional services for *Journal of Fluid Mechanics*:

Email alerts: [Click here](#)

Subscriptions: [Click here](#)

Commercial reprints: [Click here](#)

Terms of use : [Click here](#)



Particle dispersion by random waves in the rotating Boussinesq system

MIRANDA HOLMES-CERFON, OLIVER BÜHLER and RAFFAELE FERRARI

Journal of Fluid Mechanics / Volume 670 / March 2011, pp 150 - 175

DOI: 10.1017/S0022112010005240, Published online: 12 January 2011

Link to this article: http://journals.cambridge.org/abstract_S0022112010005240

How to cite this article:

MIRANDA HOLMES-CERFON, OLIVER BÜHLER and RAFFAELE FERRARI (2011). Particle dispersion by random waves in the rotating Boussinesq system. Journal of Fluid Mechanics, 670, pp 150-175 doi:10.1017/S0022112010005240

Request Permissions : [Click here](#)

Particle dispersion by random waves in the rotating Boussinesq system

MIRANDA HOLMES-CERFON^{1†},
OLIVER BÜHLER¹ AND RAFFAELE FERRARI²

¹Center for Atmosphere Ocean Science at the Courant Institute of Mathematical Sciences,
New York University, New York, NY 10012, USA

²Department of Earth, Atmospheric and Planetary Sciences, Massachusetts Institute of Technology,
Cambridge, MA 02139, USA

(Received 25 March 2010; revised 1 October 2010; accepted 4 October 2010;
first published online 12 January 2011)

We present a theoretical and numerical study of horizontal particle dispersion due to random waves in the three-dimensional rotating and stratified Boussinesq system, which serves as a simple model to study the dispersion of tracers in the ocean by the internal wave field. Specifically, the effective one-particle diffusivity in the sense of Taylor (*Proc. Lond. Math. Soc.*, vol. 20, 1921, p. 196) is computed for a small-amplitude internal gravity wave field modelled as a stationary homogeneous and horizontally isotropic Gaussian random field whose frequency spectrum is bounded away from zero. Dispersion in this system does not arise simply because of a Stokes drift effect, as in the case of surface gravity waves, but in addition it is driven by the nonlinear, second-order corrections to the linear velocity field, which can be computed using the methods of wave–mean interaction theory. A formula for the one-particle diffusivity as a function of the spectrum of the random wave field is presented. It is shown that this diffusivity is much smaller than might be expected from heuristic arguments based on the magnitude of the Stokes drift or the pseudomomentum. This appears to stem from certain incompressibility constraints for the Stokes drift and the second-order velocity field. Finally, the theory is applied to oceanic conditions described by a typical model wave spectrum, the Garrett–Munk spectrum, and also by detailed field observations from the North Atlantic tracer release experiment.

Key words: internal waves, mixing and dispersion, rotating flows

1. Introduction

That waves can disperse a collection of particles is a somewhat surprising result of fluid mechanics. A single wave is periodic, so one may naturally expect particles in a wave field to simply oscillate about their initial positions while the size of the collection remains roughly constant. However, neither the nonlinear interactions between the waves, nor the Lagrangian trajectories of particles in a wave field are purely oscillatory, and these effects combine to lead to irreversible dispersion of a collection of particles. In this paper, we study the horizontal dispersion of particles by random, small-amplitude internal waves in a three-dimensional rotating stratified fluid system, using the one-particle diffusivity of Taylor (1921) as a measure of particle

† Email address for correspondence: mholcer@seas.harvard.edu

dispersion. As is well known, a general description of the spreading of a finite-sized tracer passive tracer patch requires higher-order statistical quantities such as the two-particle diffusivity and so on, but for simplicity we restrict this paper to the easily computed one-particle diffusivity as a proxy for its multiparticle counterparts.

Our goals are twofold: first, to understand the fundamental nonlinear processes at work in this situation and, second, to apply our results to an oceanographic setting by computing the contribution that this wave-induced diffusivity can make to the horizontal dispersion of particles in the ocean interior at small horizontal scales of a few kilometres or so. We concentrate on horizontal rather than vertical dispersion, as there is a fundamental physical distinction between these in a stratified fluid at high Reynolds number. Basically, ‘horizontal’ dispersion means dispersion *along* the undulating constant-density (or constant-entropy) stratification surfaces of the fluid, whereas ‘vertical’ dispersion means dispersion *across* such surfaces. Because in an inviscid fluid stratification surfaces are materially invariant, particles can only disperse across them when there is a source of dissipation, such as wave-breaking, which leads to pockets of vigorous three-dimensional turbulence and therefore to strong viscous effects. Small-amplitude, non-breaking internal waves can contribute *only* to the horizontal dispersion, so accordingly it is only this effect that we consider.

Wave-induced horizontal dispersion has been studied in simpler two-dimensional models and the present paper builds directly on the rotating shallow-water study reported by Bühler & Holmes-Cerfon (2009, hereafter BHC). As discussed more fully in BHC, previous theoretical studies of particle dispersion by random flows fall into two categories, namely those many studies which are devoted to dispersion by a specified turbulent flow (e.g. Batchelor 1952; Kraichnan 1970; Chertkov *et al.* 1995; Majda & Kramer 1999; Sawford 2001; Toschi & Bodenschatz 2009) and those fewer studies in which the dispersion is due to random small-amplitude waves (e.g. Herterich & Hasselmann 1982; Sanderson & Okubo 1988; Weichman & Glazman 2000; Balk, Falkovich & Stepanov 2004; Balk 2006; Vucelja, Falkovich & Fouxon 2007). The crucial difference between the two cases is that in the latter, computing the relevant leading-order particle advection velocity is itself a non-trivial part of the problem, because the linear wave velocity itself produces no diffusion if there is no wave energy at zero frequency. As noted in BHC, this situation is in fact generic for gravity waves with background rotation, in which the wave frequency is bounded away from zero by the Coriolis parameter. Thus, the leading-order advection velocity arises at second order in wave amplitude, which puts the problem in the domain of wave–mean interaction theory. The task is to compute the *Lagrangian* velocity field at second order in wave amplitude, because eventually it is the zero-frequency component of this velocity field (which combines the Stokes drift and the Eulerian velocity field) that can irreversibly disperse fluid particles.

We take the velocity field to be a linear wave field at leading order and use the dynamical equations (in the form of a uniform potential vorticity constraint) to compute the second-order flow. Our study differs from the earlier internal wave study by Sanderson & Okubo (1988) by allowing for background rotation, which means that our internal waves are inertia–gravity waves. This allows us to treat waves with frequencies near the Coriolis frequency, which is essential in the ocean. The presence of background rotation makes the wave–mean interaction problem of computing the second-order advection velocity significantly more complicated because the potential vorticity constraint becomes non-trivial.

As in BHC, we model the linear wave field as a zero-mean, stationary, homogeneous Gaussian random field defined by its power spectrum. This can be obtained by

providing random Gaussian initial conditions for an internal wave field and then evolving the field in time with the usual linear equations. We restrict our analysis to fields with horizontally isotropic power spectra, which is a good starting point for internal waves in the ocean. A modelling choice has to be made with regard to the direction of vertical wave propagation in the sense of group velocity. In the ocean interior, the typical situation would be one in which upward and downward waves are equally likely, but we also consider the case in which the waves propagate predominantly in one vertical direction. It will be shown that this leads to an *increase* in the horizontal diffusivity per unit wave energy.

The wave-induced diffusivity can be thought of as arising from a particular set of wave–wave interactions, namely those in which the quadratic interactions between two waves of equal frequency project onto a zero-frequency mode of the Lagrangian flow. We consider only non-resonant wave–wave interactions and therefore only $O(1)$ time scales, although Herterich & Hasselmann (1982) and Balk & McLaughlin (1999) suggest that the projection can alternatively be interpreted as a type of resonance between two waves and two zero-frequency modes of moments of a passive scalar field. An important feature of the Boussinesq equations is that the three-dimensional dispersion relation for internal waves is scale-independent, which allows for three-dimensional equal-frequency waves with widely different spatial scales. This is in contrast with the shallow-water case, where frequency and wavelength are inextricably linked by the dispersion relation and therefore equal-frequency waves necessarily have the same horizontal wavelength. Now, as we shall see, a crucial feature of the zero-frequency horizontal Lagrangian flow is that it is constrained to be horizontally incompressible, i.e. it is area-preserving. It turns out that this constraint filters out wave–wave interactions involving waves with widely different length scales. Hence, this constraint is of little relevance in the two-dimensional case, but it severely reduces the Lagrangian flow in the three-dimensional case. Indeed, it is this constraint that renders heuristic estimates of the three-dimensional diffusivity based on wave energy or pseudomomentum amplitudes inaccurate.

Following a fundamental investigation of the three-dimensional Lagrangian flow along the lines summarized above, the main result of our study is an analytic integral expression for the diffusivity in terms of the wave power spectrum. We carefully tested our expression against numerical simulations, investigated the role of vertical propagation and the influence of the Coriolis parameter, and we established a simple exact scaling symmetry that points to the somewhat counterintuitive fact that the diffusivity increases if wave energy at a fixed frequency is moved towards *small-scale* waves. We then proceed to apply our theory to actual ocean data using the standard Garrett–Munk spectrum as well as *in situ* data obtained during the North Atlantic tracer release experiment (NATRE). The magnitude of our wave-induced diffusivity appears comparable to the magnitude of horizontal diffusion due to the so-called shear dispersion, which is often computed in ocean studies, but both processes appear to fall significantly short of accounting for the observed small-scale diffusivity of tracers at scales between 1 and 10 km in that particular tracer release experiment.

The structure of the paper is as follows. After establishing the set-up of the problem in §2, the governing equations for the second-order advection velocity are derived in §3 and some heuristic insight into the wave–mean interaction problem and the incompressibility constraint is provided in §4. The integral expression for the one-particle diffusivity is derived and analysed in §§5–6 and also tested against numerical simulations in §7. The theoretical diffusivity is then applied to situations of oceanic interest in §8 and concluding comments are given in §9.

2. Fluid equations and particle dispersion

In this section we introduce the governing equations and recall some of the definitions and structure that were laid out in more detail in BHC. We work with the standard three-dimensional rotating Boussinesq equations on an infinite domain:

$$\mathbf{u}_t + \mathbf{u} \cdot \nabla \mathbf{u} + f \hat{\mathbf{z}} \times \mathbf{u} + \nabla P = b \hat{\mathbf{z}} \quad (2.1)$$

$$b_t + \mathbf{u} \cdot \nabla b + N^2 w = 0, \quad (2.2)$$

$$\nabla \cdot \mathbf{u} = 0. \quad (2.3)$$

Here $\mathbf{x} = (x, y, z)$ are the horizontal and vertical coordinates, $\hat{\mathbf{z}}$ is the vertical unit vector, t is time, f is the Coriolis parameter, N is the buoyancy frequency, g is gravity, $\mathbf{u} = (u, v, w)$ is the velocity field, and b is the buoyancy. Both f and N are taken to be constants, which is an acceptable first approximation for small-scale ocean dynamics.

An important property of the inviscid equations is the exact material invariance of potential vorticity (PV), i.e.

$$q_t + \mathbf{u} \cdot \nabla q = 0, \quad \text{where} \quad q = (f \hat{\mathbf{z}} + \nabla \times \mathbf{u}) \cdot (N^2 \hat{\mathbf{z}} + \nabla b). \quad (2.4)$$

If the flow is spun up from rest in such a way that does not inject any potential vorticity, then q is equal to its initial value fN^2 everywhere, at all times. This gives us the exact nonlinear PV constraint

$$q = (f \hat{\mathbf{z}} + \nabla \times \mathbf{u}) \cdot (N^2 \hat{\mathbf{z}} + \nabla b) = fN^2. \quad (2.5)$$

We seek solutions to (2.1)–(2.3) as an asymptotic expansion in powers of a small-amplitude parameter $a \ll 1$. We assume no motion at leading order, so the $O(1)$ velocity and buoyancy fields are zero. In standard notation, the solution takes the form

$$\begin{pmatrix} \mathbf{u} \\ b \end{pmatrix} = \begin{pmatrix} \mathbf{0} \\ 0 \end{pmatrix} + a \begin{pmatrix} \mathbf{u}_1 \\ b_1 \end{pmatrix} + a^2 \begin{pmatrix} \mathbf{u}_2 \\ b_2 \end{pmatrix} + O(a^3). \quad (2.6)$$

This regular perturbation expansion can be expected to be valid for an $O(1)$ time scale as $a \rightarrow 0$. We take the $O(a)$ flow to be a stationary, homogeneous, horizontally isotropic Gaussian random wave field constrained to satisfy the linearized versions of (2.1)–(2.3), and we make the additional assumption that the power spectrum of the waves is bounded away from zero. If $f \neq 0$, then it can be seen from the linear dispersion relation (2.14) that this constraint is satisfied automatically, but if $f = 0$ then this is an additional constraint on the energy spectrum.

As a measure of diffusion, we use a particle-based measure introduced by Taylor (1921), which associates a diffusivity with the displacement variance of a particle, so that $D_{ij} = (1/2)(d/dt)\mathbb{E}[(X_i(t) - X_i(0))(X_j(t) - X_j(0))]$, where X_j is the j th Cartesian component of the Lagrangian velocity field, and \mathbb{E} is the expectation over realizations of the random velocity field. In our case, the vertical components of the diffusion tensor are zero and the horizontal components are isotropic, with each component equal to

$$D_u \equiv \int_0^\infty C_{u,u}(\tau) d\tau = \frac{1}{2} \hat{C}_{u,u}(0), \quad \text{where} \quad C_{u,u}(\tau) \equiv \mathbb{E}[\overline{u(t)}u(t+\tau)] \quad (2.7)$$

is the correlation function of u , an arbitrary Cartesian component of the Lagrangian velocity vector, the power spectrum $\hat{C}_{u,u}(\omega)$ is its Fourier transform, and the overbar denotes complex conjugation. Clearly, only the value of the power spectrum at $\omega = 0$ is relevant for the diffusivity.

As noted in BHC, if the velocity field contains a component that is the time derivative of a stationary random field, then this component does not contribute to the diffusivity. To be specific, if $u = U + V_t$, where U and V are stationary random variables, V is differentiable, and their correlation and cross-correlation functions decay at temporal infinity, then

$$D_u = D_U. \quad (2.8)$$

Henceforth we will use the symbol $\stackrel{t}{=}$ to mean ‘equal up to a time derivative of a stationary function’, so $u \stackrel{t}{=} U$ in the present example.

2.1. Random linear waves modelled as a Gaussian process

The linear velocity field can be written as a stochastic Fourier integral; the details of this are slightly technical and are spelled out in a simple pedagogical example in BHC. The result is

$$\begin{pmatrix} u_1 \\ v_1 \\ w_1 \\ b_1 \end{pmatrix} = \frac{1}{(2\pi)^4} \int \exp(i(kx + ly + mz + \omega t)) \begin{pmatrix} \left(\cos \theta - i \frac{f}{\omega} \sin \theta \right) \sin \beta \\ \left(\sin \theta + i \frac{f}{\omega} \cos \theta \right) \sin \beta \\ -\cos \beta \\ -i \frac{N^2}{\omega} \cos \beta \end{pmatrix} d\hat{\phi}, \quad (2.9)$$

where $d\hat{\phi}$ is a random measure on the dual space $\{\mathbf{K} = (k, l, m, \omega) \in \mathbb{R}^{4*}\}$, such that

$$\mathbb{E}[d\hat{\phi}(\mathbf{K})] = 0, \quad \overline{d\hat{\phi}(\mathbf{K})} = d\hat{\phi}(-\mathbf{K}), \quad (2.10)$$

$$\mathbb{E}[\overline{d\hat{\phi}(\mathbf{K})} d\hat{\phi}(\mathbf{K}')] = (2\pi)^4 E(\mathbf{K}) \delta(\mathbf{K} - \mathbf{K}') dk dk' dl dl' dm dm' d\omega d\omega'. \quad (2.11)$$

The spatial Fourier coordinates are sometimes written using spherical variables (K, β, θ) , where $K^2 = k^2 + l^2 + m^2$, $\beta \in [-\pi/2, \pi/2]$ is the vertical angle such that $m = K \sin \beta$, and $\theta \in [0, 2\pi)$ is the horizontal angle. The density $E(\mathbf{K}) = E(-\mathbf{K})$ is normalized such that the expected value of the linear energy density per unit volume is given by

$$\bar{E} = \frac{1}{2} \mathbb{E} \left[|u_1|^2 + |v_1|^2 + |w_1|^2 + \frac{|b_1|^2}{N^2} \right] = \frac{1}{(2\pi)^4} \int E(\mathbf{K}) dk dl dm d\omega. \quad (2.12)$$

We will consider only wave fields that are horizontally isotropic and to simplify notation we will denote spectral densities with respect to different variables by the same symbol. For example, when converting $E(\mathbf{K})$ into spherical coordinates, we write

$$E(\mathbf{K}) dk dl dm d\omega = E(K, \beta, \omega) dK d\beta d\theta d\omega, \quad \text{so } E(\mathbf{K}) K^2 \cos \beta = E(K, \beta, \omega). \quad (2.13)$$

The wave field satisfies the linear equations, so $E(\mathbf{K})$ is supported only on surfaces $\omega = \pm \omega(k, l, m)$, where the positive branch of the dispersion relation is

$$\omega(k, l, m) = \sqrt{\frac{N^2(k^2 + l^2) + f^2 m^2}{k^2 + l^2 + m^2}} \Leftrightarrow \omega(\beta) = \sqrt{N^2 \cos^2 \beta + f^2 \sin^2 \beta}. \quad (2.14)$$

Thus, $E(\mathbf{K})$ consists of terms proportional to $\delta(\omega \pm \omega(\beta))$. As mentioned before, a modelling assumption needs to be made regarding the vertical

structure of the waves. One approach is to write the entire wave field as a combination of standing waves in the vertical (e.g. Sanderson & Okubo 1988), although this makes the wave field inhomogeneous in the vertical. We prefer to allow for independent upward and downward propagating waves in the sense of vertical group velocity, which for internal waves has the opposite sign as the vertical phase velocity (e.g. Lighthill 1978). Based on the phase convention in (2.9), the sign of the vertical group velocity is equal to $\text{sgn}(m\omega) = \text{sgn}(\beta\omega)$, so we adopt the representation

$$E(\mathbf{K}) = E_{up}(\mathbf{K}) + E_{down}(\mathbf{K}) \quad (2.15)$$

with

$$E_{up}(K, \beta, \omega) = \pi S_{up}(K, |\beta|)(\delta(\omega - \omega(\beta)) + \delta(\omega + \omega(\beta)))1_{\text{sgn}(\beta)=\text{sgn}(\omega)}, \quad (2.16)$$

$$E_{down}(K, \beta, \omega) = \pi S_{down}(K, |\beta|)(\delta(\omega - \omega(\beta)) + \delta(\omega + \omega(\beta)))1_{\text{sgn}(\beta)=-\text{sgn}(\omega)}. \quad (2.17)$$

Here 1_x is the indicator function that is unity if x is true and zero otherwise, and $S_{up}(K, \beta)$, $S_{down}(K, \beta)$ are defined for $\beta > 0$ and are normalized such that

$$\frac{1}{(2\pi)^2} \int_{K>0, \beta>0} S_{up} dK d\beta = \bar{E}_{up}, \quad \frac{1}{(2\pi)^2} \int_{K>0, \beta>0} S_{down} dK d\beta = \bar{E}_{down}. \quad (2.18)$$

We will ultimately work with spectra defined on total wavenumber K and positive frequency ω ; as in (2.13), the corresponding density can be obtained via

$$S_{up,down}(K, \omega) dK d\omega = S_{up,down}(K, \beta) dK d\beta. \quad (2.19)$$

This completes the specification of the random linear wave field.

3. The second-order Lagrangian velocity

Taylor's formula (2.7) for the diffusivity requires the Lagrangian velocity of a particle, which, to leading-order, is simply the Eulerian field at $O(a)$. However, if the power spectrum of the wave field is zero at $\omega=0$, then this $O(a)$ wave field does not contribute to the particle diffusivity. In this case, the leading-order diffusivity stems from the $O(a^2)$ Lagrangian velocity field, which is not given *a priori*.

The $O(a^2)$ Lagrangian velocity field is a sum of two parts, namely

$$\mathbf{u}_2^L = \mathbf{u}_2 + \mathbf{u}_2^S, \quad \text{where} \quad \mathbf{u}_2^S = (\boldsymbol{\xi}_1 \cdot \nabla) \mathbf{u}_1 \quad (3.1)$$

is the Stokes drift, a Lagrangian correction that accounts for the variations in the velocity field that the particle encounters as it oscillates around its mean position. It is defined using $\boldsymbol{\xi}_1$, which is the usual linear particle displacement field such that $\partial_t \boldsymbol{\xi}_1 = \mathbf{u}_1$. The other term, \mathbf{u}_2 , is an Eulerian correction, which comes from the fact that a superposition of linear waves is not an exact solution to the Boussinesq equations, so the nonlinear advection terms will generate flow at higher orders.

We would like to find an expression for \mathbf{u}_2^L in terms of the linear wave field. The Stokes drift is already in such a form, so one approach for finding such an expression is to solve for \mathbf{u}_2 via brute force expansion and manipulation of the Boussinesq equations and the PV constraint at $O(a^2)$, as was done in BHC. Alternatively, one can use particle labels and the Lagrangian fluid equations as given by Lamb (1932) as a basis for an asymptotic expansion. This approach was pursued by Sanderson & Okubo (1988) for non-rotating internal waves, and it is possible to extend their calculation to rotating fluids provided that a suitable Lagrangian version of the PV constraint (2.5) is incorporated.

We found it convenient to build our approach on Bühler & McIntyre (1998, hereafter BM), who used the framework of generalized Lagrangian-mean (GLM) theory introduced by Andrews & McIntyre (1978). GLM theory avoids the use of particle labels and it provides exact equations for the Lagrangian-mean velocity, the pseudomomentum and the Lagrangian-mean PV, which together can then be exploited in the PV constraint (see Bühler 2009 for more information on the wave-mean interaction theory). Of course, all approaches must lead to the same \mathbf{u}_2^L in the end, so our choice of GLM theory merely facilitates the computation of \mathbf{u}_2^L . Notably, we will use the GLM formalism without an explicit averaging operator (hence we write \mathbf{u}_2^L instead of $\bar{\mathbf{u}}_2^L$), but one can regard the projection onto the $O(a^2)$ part of the expansion as the definition of the mean flow in the present context. Hence, the ‘mean’ flow in the present context is still a random flow.

3.1. Low-frequency equations for the Lagrangian velocity

We work at $O(a^2)$ and seek to focus attention on the low-frequency part of \mathbf{u}_2^L , which contains the frequencies in the neighbourhood of zero that are relevant for dispersion. The $O(a^2)$ GLM equations for constants f and N and with zero $O(1)$ mean flow are (cf. (9.23) and (9.24) of BM)

$$\partial_t(\nabla \times (\mathbf{u}_2^L - \mathbf{p}_2)) + f\hat{\mathbf{z}}\nabla \cdot \mathbf{u}_2^L - (f\hat{\mathbf{z}} \cdot \nabla)\mathbf{u}_2^L = \nabla b_2^L \times \hat{\mathbf{z}} \quad (3.2)$$

$$\partial_t b_2^L + N^2 w_2^L = 0, \quad (3.3)$$

where the GLM pseudomomentum vector \mathbf{p}_2 has Cartesian components

$$p_{2i} = -\xi_{1j,i} (u_{1,j} + [f\hat{\mathbf{z}} \times \boldsymbol{\xi}_1]_j) \quad (3.4)$$

and summation over repeated indices is implied. For incompressible flow, $\nabla \cdot \mathbf{u} = 0$ but $\nabla \cdot \mathbf{u}_2^L \neq 0$; this is the divergence effect of the Lagrangian-mean flow. Specifically,

$$\nabla \cdot \mathbf{u}_2^L = \frac{1}{2} \partial_t (\xi_{1i} \xi_{1j})_{,ij}. \quad (3.5)$$

We can now make good use of (2.8) to simplify (3.2)–(3.5):

$$-f \frac{\partial \mathbf{u}_2^L}{\partial z} \stackrel{!}{=} \nabla b_2^L \times \hat{\mathbf{z}}, \quad w_2^L \stackrel{!}{=} 0, \quad \text{and} \quad \nabla^H \cdot \mathbf{u}_2^L \stackrel{!}{=} 0, \quad (3.6)$$

where $\nabla^H = (\partial_x, \partial_y, 0)$. Thus, the low-frequency Lagrangian-mean flow is horizontal and has the familiar structure of a balanced flow, which can be described by a quasi-geostrophic streamfunction ψ^L such that

$$u_2^L = -\psi_y^L, \quad v_2^L = \psi_x^L, \quad w_2^L = 0, \quad b_2^L = f\psi_z^L. \quad (3.7)$$

Clearly, $w_2^L \stackrel{!}{=} 0$ implies that the vertical diffusivity is zero, as discussed in §1.

In order to find an equation for ψ^L , we turn to the PV constraint. It is a particular strength of GLM theory that it is possible to write down an exact expression of the Lagrangian-mean PV ((9.18) in BM; Bühler 2009). In the present case, this yields

$$q^L = \frac{(\nabla \times (\mathbf{u}^L - \mathbf{p}) + f\hat{\mathbf{z}}) \cdot \nabla (b^L + N^2 z)}{\tilde{\rho}} = fN^2, \quad (3.8)$$

where $\tilde{\rho}$ solves $\partial_t \tilde{\rho} + \nabla \cdot (\tilde{\rho} \mathbf{u}^L) = 0$. The latter can be expanded in amplitude as $\tilde{\rho} = 1 + a^2 \tilde{\rho}_2 + O(a^3)$, where $\tilde{\rho}_2 = -(1/2)(\xi_{1,i} \xi_{1,j})_{,ij}$ by (3.5). At $O(a^2)$, the PV constraint becomes

$$N^2 \hat{\mathbf{z}} \cdot \nabla \times (\mathbf{u}_2^L - \mathbf{p}_2) + f \frac{\partial b_2^L}{\partial z} + \frac{1}{2} f N^2 ((\xi_{1,i} \xi_{1,j})_{,ij}) = 0. \quad (3.9)$$

Substituting the streamfunction and using $\nabla \cdot \xi_1 = 0$ leads to

$$\left(\Delta^H + \frac{f^2}{N^2} \partial_{zz} \right) \psi^L \stackrel{t}{=} \hat{\mathbf{z}} \cdot (\nabla \times \mathbf{p}_2) - \frac{1}{2} f \nabla \cdot (\xi_1 \cdot \nabla \xi_1), \quad (3.10)$$

where Δ^H is the horizontal Laplacian. This differs from the equation considered in BM by the last term, which was negligible in the context of a slowly varying wavetrain considered there. However, this term is important for Gaussian random waves. Equation (3.10) is the fundamental relation that we will use to solve for \mathbf{u}_2^L at low frequency.

4. Heuristic analysis of the incompressibility constraint

As noted in §1, the incompressibility constraint (3.6) for the horizontal Lagrangian flow plays a crucial role in limiting the diffusivity D for three-dimensional flows. This important fact is easily obscured in the detailed computation of D that follows below, so we provide a heuristic discussion of the issue here in the non-rotating case $f = 0$. This is essentially the physical situation studied by Sanderson & Okubo (1988), and in this case (3.10) reduces to

$$\Delta^H \psi^L = \hat{\mathbf{z}} \cdot \nabla \times \mathbf{u}_2^L \stackrel{t}{=} \hat{\mathbf{z}} \cdot \nabla \times \mathbf{p}_2 \quad \text{and} \quad \nabla^H \cdot \mathbf{u}_2^L \stackrel{t}{=} 0. \quad (4.1)$$

Hence, at every altitude z , the horizontal Lagrangian-mean flow is simply the least-squares projection of the horizontal pseudomomentum onto horizontally non-divergent vector fields; this is the incompressibility constraint in its purest form. The question to understand is how important is this constraint, e.g. how wrong would D be if one approximated (4.1) by $\mathbf{u}_2^L \stackrel{t}{=} \mathbf{p}_2$ for the horizontal flow components?

We will investigate (4.1) and this question by looking at the extreme case of one or two plane waves; the general case can then be built up by integrating over a continuum of all possible wave modes. To make this heuristic analysis as simple as possible we will ignore the vertical direction completely in this section, so all vectors and gradient operators will be horizontal only. This is quantitatively correct for hydrostatic internal waves and makes the equations similar to those governing the non-rotating shallow-water system. We will also omit the expansion subscripts.

4.1. Self-interaction of a single plane wave

A single plane wave with amplitude A has the horizontal velocity and displacement fields

$$\mathbf{u} = A \frac{\mathbf{k}}{\kappa} \cos \theta \quad \text{and} \quad \xi = -A \frac{\mathbf{k}}{\omega \kappa} \sin \theta. \quad (4.2)$$

Here \mathbf{k} is the horizontal wavenumber vector, $\kappa = |\mathbf{k}|$ is its magnitude, ω is its frequency, and $\theta(\mathbf{x}, t)$ is the wave phase such that $\mathbf{k} = \nabla \theta$ and $\omega = -\theta_t$. Importantly, we assume $\omega > 0$ and with this convention (this differs from the convention used in (2.9)) \mathbf{k} points in the direction of horizontal propagation of the wave. The corresponding pseudomomentum vector from (3.4) is

$$\mathbf{p} = -(\nabla \xi) \cdot \mathbf{u} = \frac{A^2}{2} \frac{\mathbf{k}}{\omega} (\cos 2\theta + 1). \quad (4.3)$$

Hence, \mathbf{p} points in the direction of \mathbf{k} and its space-time structure consists of an oscillatory part with wavenumber vector $2\mathbf{k}$ and frequency 2ω plus a constant part. The oscillatory part does not project onto zero frequency and can therefore be ignored,

i.e. $\cos 2\theta \stackrel{t}{=} 0$. The constant gives rise to the generic expression $\mathbf{p} = \mathbf{k}/\omega E$ for the pseudomomentum of a plane wave in terms of the local energy density $E = A^2/2$. This constant pseudomomentum has zero curl and therefore $\Delta^H \psi^L = 0$ in (4.1), which implies $\nabla \psi^L = 0$ and therefore $\mathbf{u}^L = 0$ if periodic boundary conditions are applied to ψ^L . In the approximation $\mathbf{u}^L = \mathbf{p}$, the constant pseudomomentum would give rise to a uniform motion of the fluid layer as a whole, which however does not disperse particle clouds. Either way, we obtain no particle diffusion and therefore we conclude that the pseudomomentum of a single plane wave is ignorable for diffusion.

4.2. Pair interaction of two plane waves

We now consider two different plane waves with respective amplitudes A_1 and A_2 , say, and analogous notation for the other parameters. The quadratic pseudomomentum $\mathbf{p} = \mathbf{p}_{11} + \mathbf{p}_{12} + \mathbf{p}_{21} + \mathbf{p}_{22}$, where the subscripts denote the wave used to evaluate ξ and \mathbf{u} in (4.3), e.g. $\mathbf{p}_{12} = -(\nabla \xi_1) \cdot \mathbf{u}_2$. The same-wave components \mathbf{p}_{11} and \mathbf{p}_{22} are ignorable for particle diffusion by the arguments given in §4.1. The mixed-wave components are

$$\mathbf{p}_{12} + \mathbf{p}_{21} = \frac{A_1 A_2 \cos \alpha_{12}}{2} \left(\frac{\mathbf{k}_1}{\omega_1} + \frac{\mathbf{k}_2}{\omega_2} \right) (\cos(\theta_1 + \theta_2) + \cos(\theta_1 - \theta_2)), \quad (4.4)$$

where α_{12} is the angle between \mathbf{k}_1 and \mathbf{k}_2 . Now, the sum term $\cos(\theta_1 + \theta_2)$ has wavenumber vector $\mathbf{k}_1 + \mathbf{k}_2$ and frequency $\omega_1 + \omega_2$, which is always non-zero. Hence, $\cos(\theta_1 + \theta_2) \stackrel{t}{=} 0$ and this term is ignorable for diffusion. On the other hand, the difference term $\cos(\theta_1 - \theta_2)$ can have zero frequency if $\omega_1 = \omega_2$. In this case, we have

$$\mathbf{p}_{12} + \mathbf{p}_{21} \stackrel{t}{=} \frac{A_1 A_2 \cos \alpha_{12}}{2\omega_1} (\mathbf{k}_1 + \mathbf{k}_2) \cos(\theta_1 - \theta_2). \quad (4.5)$$

The divergent part of this pseudomomentum field does not contribute to \mathbf{u}^L , and we can extract that part by projecting (4.5) onto the associated wavenumber vector $\mathbf{k}_1 - \mathbf{k}_2$. This yields

$$\frac{A_1 A_2 \cos \alpha_{12}}{2\omega_1} \frac{(\mathbf{k}_1 + \mathbf{k}_2) \cdot (\mathbf{k}_1 - \mathbf{k}_2)}{|\mathbf{k}_1 - \mathbf{k}_2|} \cos(\theta_1 - \theta_2) \propto \kappa_1^2 - \kappa_2^2. \quad (4.6)$$

Therefore, we obtain the important result that the magnitude of the divergent part of (4.5) is proportional to the difference of the horizontal wavenumber magnitudes.

In non-rotating shallow water, the dispersion relation is $\omega = c\kappa$ and therefore $\omega_1 = \omega_2$ implies that $\kappa_1 = \kappa_2$. Hence, in this case the zero-frequency pseudomomentum in (4.4) is non-divergent and therefore equal to the zero-frequency mean flow \mathbf{u}^L . In other words, the incompressibility constraint (4.1) is automatically satisfied in the shallow-water system.

On the other hand, for internal waves the frequency condition $\omega_1 = \omega_2$ does not imply $\kappa_1 = \kappa_2$, because by (2.14) the frequency depends on the *ratio* of κ to the vertical wavenumber m , so we only have the weaker statement $\kappa_1/m_1 = \kappa_2/m_2$. We conclude that for internal waves with widely different horizontal wavelengths, the incompressibility constraint severely reduces the magnitude of the diffusive component of \mathbf{u}^L , which is therefore mostly due to interactions of waves with comparable horizontal wavelengths. We will rediscover this dominance of equal-wavelength interactions in §5.3.

With these results in hand, we can now answer the question posed at the beginning of this section. Namely, in the non-rotating shallow-water system one could set $\mathbf{u}^L \stackrel{t}{=} \mathbf{p}$ with no error in D , whilst in the three-dimensional Boussinesq system the

same approximation would lead to overestimating D : the incompressibility constraint is important in the three-dimensional case.

Despite the heuristic utility of considering a few plane waves, one should be aware of the practical limitations of this approach. First, the simple explicit results are limited to non-rotating flow and, second, the results written for finite amplitudes A_1 and A_2 would need to be interpreted in the sense of distributions, because a realistic wave field cannot have a finite amount of energy in any particular plane wave component. This is also obvious from the zero-frequency \mathbf{u}^L computed above: any *finite* steady mean flow would lead to ballistic particle trajectories and not to diffusion. This is in fact a practical problem for numerical simulations of wave fields in a large but finite periodic domain, which use discrete Fourier series and finite wave amplitudes. In such simulations, the particle trajectory in any given realization deviates at very long times from that predicted for an unbounded domain because of the presence of a weak but non-zero steady flow field.

Nevertheless, with these caveats understood, it is true that the detailed technical computations for D that follow are essentially straightforward extensions of the present heuristic analysis to rotating flows and to a continuum of wave modes.

5. Diffusivity calculation

The task is now to compute the covariance functions $C_{u_2^L, u_2^L}$, $C_{v_2^L, v_2^L}$, and to integrate each in time at a fixed point in space to obtain the horizontal diffusivity. Recognizing that $C_{u_2^L, u_2^L} = -(\partial^2/\partial y^2)C_{\psi^L, \psi^L}$, $C_{v_2^L, v_2^L} = -(\partial^2/\partial x^2)C_{\psi^L, \psi^L}$, we find it easier to calculate the diffusivity from the expression

$$2D = C_{u_2^L, u_2^L} + C_{v_2^L, v_2^L} = \frac{1}{2} \int_{-\infty}^{\infty} -\Delta^H C_{\psi^L, \psi^L} dt \quad (5.1)$$

evaluated at zero spatial lag. Without any simplifying assumptions, when the integrand is written in Fourier space, this is a 17-dimensional integral of a somewhat lengthy expression. We will be able to reduce this to a three-dimensional integral by manipulations that, *mutatis mutandis*, mirror the shallow-water manipulations in §4.3 in BHC. We will outline the derivation of our final result, but will keep the expressions concise by representing the integrands using abstract function symbols and relegating the actual algebraic expressions to the Appendix.

5.1. Deriving the diffusivity integral

First, we use (3.10) to express ψ^L in Fourier space as an eight-dimensional stochastic integral:

$$\psi^L(\mathbf{X}) = \frac{1}{(2\pi)^8} \int \gamma(\mathbf{K}_1, \mathbf{K}_2) \exp(i\mathbf{X} \cdot (\mathbf{K}_1 + \mathbf{K}_2)) d\hat{\phi}_1 d\hat{\phi}_2. \quad (5.2)$$

Here $\mathbf{X} = (x, y, z, t)$ is the dual of $\mathbf{K} = (k, l, m, \omega)$. It follows that

$$C_{\psi^L, \psi^L}(\mathbf{X}) = \frac{1}{(2\pi)^{16}} \int \gamma(\mathbf{K}_1, \mathbf{K}_2) \overline{\gamma(\mathbf{K}_3, \mathbf{K}_4)} \exp(i\mathbf{X} \cdot (\mathbf{K}_1 + \mathbf{K}_2)) \mathbb{E}[d\hat{\phi}_1 d\hat{\phi}_2 \overline{d\hat{\phi}_3 d\hat{\phi}_4}]. \quad (5.3)$$

Now we invoke the assumption of a Gaussian random field to expand the fourth moment as a sum of second moments (see BHC for more details). Each of these

contains a δ -function singularity from (2.11), which we can integrate over to get

$$C_{\psi^L, \psi^L} = \frac{1}{(2\pi)^8} \int (|\gamma(\mathbf{K}_1, \mathbf{K}_2)|^2 + \gamma(\mathbf{K}_1, \mathbf{K}_2)\overline{\gamma(\mathbf{K}_2, \mathbf{K}_1)})E(\mathbf{K}_1)E(\mathbf{K}_2) \\ \times \exp(i(\mathbf{K}_1 + \mathbf{K}_2) \cdot \mathbf{X}) d\mathbf{K}_1 d\mathbf{K}_2. \quad (5.4)$$

Switching the labels (1,2) and averaging the resulting integrands yields a symmetric expression that is easier to deal with. Taking the negative horizontal Laplacian gives

$$-\Delta^H C_{\psi^L, \psi^L}(\mathbf{X}) = \frac{1}{(2\pi)^8} \int g(\mathbf{K}_1, \mathbf{K}_2)E(\mathbf{K}_1)E(\mathbf{K}_2) \exp(i\mathbf{X} \cdot (\mathbf{K}_1 + \mathbf{K}_2)) d\mathbf{K}_1 d\mathbf{K}_2, \quad (5.5)$$

where

$$g(\mathbf{K}_1, \mathbf{K}_2) = g(\mathbf{K}_2, \mathbf{K}_1) = \frac{(k_1 + k_2)^2 + (l_1 + l_2)^2}{2} |\gamma(\mathbf{K}_1, \mathbf{K}_2) + \gamma(\mathbf{K}_2, \mathbf{K}_1)|^2. \quad (5.6)$$

Using (5.1), the one-particle diffusivity at $x = y = z = 0$ is

$$4D = \frac{1}{(2\pi)^8} \int g(\mathbf{K}_1, \mathbf{K}_2)E(\mathbf{K}_1)E(\mathbf{K}_2) \exp(i(\omega_1 + \omega_2)t) d\mathbf{K}_1 d\mathbf{K}_2 dt. \quad (5.7)$$

We now switch to spherical wavenumber coordinates such that

$$g(\mathbf{K}_1, \mathbf{K}_2) = g(K_1, \beta_1, \theta_1, \omega_1, K_2, \beta_2, \theta_2, \omega_2) \quad (5.8)$$

and then we exploit several δ -function singularities. First, time integration replaces $\exp(i(\omega_1 + \omega_2)t)$ with $2\pi\delta(\omega_1 + \omega_2)$ and integration over ω_2 then replaces ω_2 by $-\omega_1$ in all terms. Using (2.15)–(2.17) then brings in four products of δ -functions involving ω_1 , but two of them are equal to zero in distribution because the dispersion function $\omega(\beta) > 0$ by definition. Integrating over ω_1 and a few more steps detailed in the Appendix (§ A.1) then lead to

$$4D = \frac{1}{(2\pi)^4} \int_{\omega>0} \{(S_{up}(K_1, \omega)S_{up}(K_2, \omega) + S_{down}(K_1, \omega)S_{down}(K_2, \omega))G_2 \\ + (S_{up}(K_1, \omega)S_{down}(K_2, \omega) + S_{down}(K_1, \omega)S_{up}(K_2, \omega))G_1\} dK_1 dK_2 d\theta d\omega, \quad (5.9)$$

where the integral is over positive ω only and

$$\left. \begin{aligned} G_1(K_1, K_2, \omega, \theta) &= \frac{1}{2}g(K_1, \beta(\omega), \theta_1, \omega, K_2, \beta(\omega), \theta_2, -\omega), \\ G_2(K_1, K_2, \omega, \theta) &= \frac{1}{2}g(K_1, \beta(\omega), \theta_1, \omega, K_2, -\beta(\omega), \theta_2, -\omega). \end{aligned} \right\} \quad (5.10)$$

Explicit expressions for G_1 and G_2 are given in the Appendix (§ A.2). Here the function $\beta(\omega) > 0$ for $\omega > 0$ is the inverse of the dispersion relation (2.14), and $\theta = \theta_1 - \theta_2$. Because of the rotational symmetry of the governing equations, each of G_1, G_2 depends only on $\theta_1 - \theta_2$, so we have simplified (5.9) by replacing this difference with a single variable and integrating over the extra angle variable. Note that $G_1 \neq G_2$ in general; this is discussed in § 5.2.

Finally, for horizontally isotropic spectra we can reduce (5.9) to the three-dimensional integral

$$D = \frac{1}{4} \frac{1}{(2\pi)^3} \int_{\omega>0} \{(S_{up}(K_1, \omega)S_{up}(K_2, \omega) + S_{down}(K_1, \omega)S_{down}(K_2, \omega))H_2 \\ + (S_{up}(K_1, \omega)S_{down}(K_2, \omega) + S_{down}(K_1, \omega)S_{up}(K_2, \omega))H_1\} dK_1 dK_2 d\omega, \quad (5.11)$$

where the diffusivity densities $H_i(K_1, K_2, \omega) = (1/2\pi) \int G_i d\theta$. This is our fundamental theoretical result for the diffusivity D , analogous to the one-dimensional integral

(4.24) in BHC. It illustrates that for each ω the diffusivity D receives contributions from wave pairs with all possible wavenumber magnitudes K_1 and K_2 , as expected from §4.

In the following sections, we analyse the diffusivity densities H_i , as these are the lowest-dimensional functions that exactly determine the properties of the diffusivity for horizontally isotropic spectra. However, while we have calculated the exact analytic expressions for the functions with a symbolic integrator, the expressions are far too large to reproduce, and in practice one must use (5.9) to calculate diffusivities numerically.

5.2. Upward and downward waves

Equation (5.11) makes obvious that it matters for D whether the wave spectrum consists of waves all going in the same vertical direction, or whether the wave spectrum is distributed into a mixture of upward and downward waves. Over a large parameter range including that of primary oceanic interest, we find that H_1 multiplying the mixed-direction terms in (5.11) is negligible compared to H_2 , which multiplies the same-direction terms. Hence, a spectrum with waves going entirely in one vertical direction produces about twice the diffusivity as the same spectrum equally divided between the vertical directions.

To analyse this point, we first observe that if there is equal energy in waves going up and waves going down, then the integrand in (5.11) is proportional to $H_0 = (H_1 + H_2)/2$, whereas in the limit of all the waves going in the same vertical direction, the same term approaches H_2 . Therefore, it is the relative size of H_1 and H_2 that matters. The analytic expressions for these functions are very cumbersome unless $f = 0$ (see §A.2 for the forms of the H_i in this case), but they can be easily evaluated numerically. To aid this process, we first non-dimensionalize the functions by defining the non-dimensional variables

$$r = \min \left\{ \frac{K_1}{K_2}, \frac{K_2}{K_1} \right\}, \quad s = \frac{\omega - f}{N - f}, \quad a = \frac{f}{N}. \quad (5.12)$$

Here $r \leq 1$ is a scale parameter, which shows the contribution to the diffusivity from waves of different scales; s is a frequency parameter, defined by mapping the allowable range of frequencies $[f, N]$ linearly onto the interval $[0, 1]$; and a is the Prandtl ratio. For oceanic applications, both s and a are typically significantly smaller than unity. We can write H_i in terms of a non-dimensional function h_i as

$$H_i(K_1, K_2, \omega) = \max \{K_1^2, K_2^2\} h_i(r, s, a)/N^2. \quad (5.13)$$

This makes explicit that H_i are homogeneous of degree two in the wavenumber magnitudes, i.e.

$$H_i(\alpha K_1, \alpha K_2, \omega) = \alpha^2 H_i(K_1, K_2, \omega) \quad (5.14)$$

for any constant $\alpha > 0$. We will use this property in §6.2.

The functions $h_i \geq 0$ are maximized by their values at $r = 1$, with fairly rapid decay away from this value (see figure 2). This means that for each ω , the main contribution to D in (5.11) stems from the wavenumber regions in which $K_1 \approx K_2$. This is consistent with the heuristic pseudomomentum arguments in §4.2, because at fixed ω this condition implies that the *horizontal* wavenumber magnitudes are also comparable, which was the crucial criterion for the pseudomomentum to project well onto a non-divergent mean flow. We restrict attention to $r \approx 1$, and in figure 1 the two functions h_1 and h_2 are compared for this value. The plots show that $h_2(1, s, a) \geq h_1(1, s, a)$ everywhere, and indeed, $h_1 \approx 0$ except when s is near 1 or

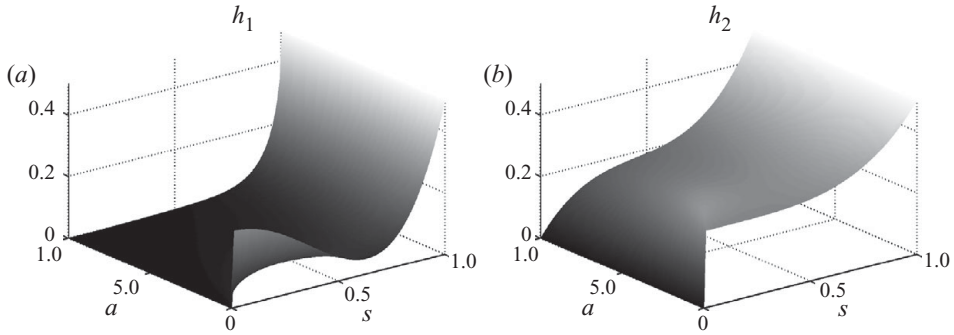


FIGURE 1. Non-dimensional diffusivity densities (a) $h_1(1, s, a)$ for waves travelling in opposite vertical directions and (b) $h_2(1, s, a)$ for waves in the same vertical direction.

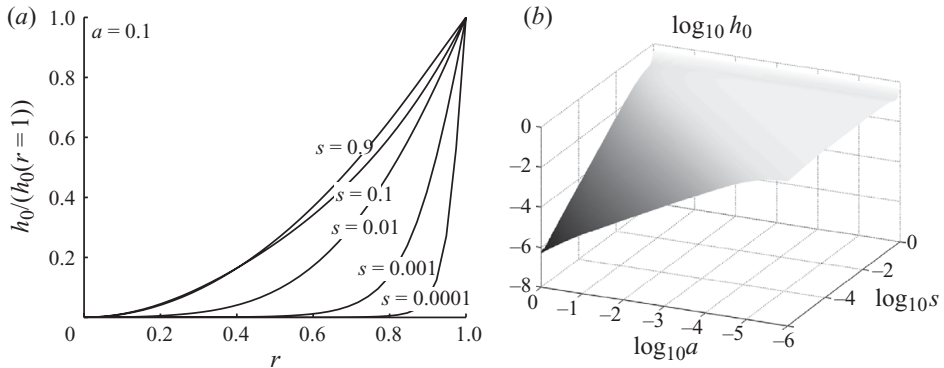


FIGURE 2. (a) $h_0(r, s, a=0.1)/h_0(1, s, a=0.1)$ for several different values of s as a function of r , the ratio of interacting wavenumbers. The density decreases roughly quadratically in r for large s (frequencies away from the inertial frequency), but drops off much more sharply for small s . (b) The non-dimensional diffusivity density $h_0(1, s, a)$ in log space for spectra with equal energy in waves travelling in each vertical direction.

when $a=0$, which is the case of zero rotation. Therefore, it appears that for oceanic applications, where Coriolis effects are important and there is very little energy near the buoyancy frequency, the contribution of h_1 is negligible; we continue to include it here for generality.

5.3. Influence of scale separation and rotation

We restrict to the up-down symmetric case of vertical wave propagation such that the relevant non-dimensional diffusivity density is $h_0 = 0.5(h_1 + h_2)$. First, we look at the contribution from waves of different spatial scales. In figure 2, we plot $h_0(r, s, a=0.1)/h_0(1, s, a=0.1)$ as a function of r for several different values of s , to illustrate how the diffusivity drops off sharply as a function of the scale separation of the interacting waves. We show this for only one particular value of a but the results are the same for the many values we have tested. In a little more detail, we have found from the log-log plots (not shown) that when $s \gtrsim a$, the diffusivity density is very close to a quadratic function of r over the full range of r and therefore

$$h_0(r, s, a) \approx r^2 h_0(1, s, a). \quad (5.15)$$

When $s \ll a$, i.e. when $\omega - f \ll f$, the diffusivity density drops off more sharply near $r = 1$, but then becomes quadratic again for small values of r .

Next, we look at the frequency-dependence of h_0 to discern the importance of rotation. As illustrated in figure 2, there is only a weak dependence on $a = f/N$ away from $a = 0$, so we need to only consider how h_0 varies with the scaled frequency variable s . Basically, over most of its range, h_0 is approximately 0.17, rising to 0.5 for frequencies near N and dropping to zero for frequencies near f . We can Taylor-expand $h_0(1, s, a)$ about $s = 0$ to find the linear coefficient as $s \rightarrow 0$, and the result is

$$h_0(1, s, a) = \frac{s}{a(1+a)} + O(s^2) \approx \frac{\omega - f}{f} \quad (s \rightarrow 0). \quad (5.16)$$

In the last approximation, we assumed $a = f/N \ll 1$, as is the case in much of the ocean. The apparent reduction of h_0 near the Coriolis frequency is reminiscent of the strong suppression of diffusion by Coriolis effects found previously in the shallow-water analysis of BHC. Conversely, in the non-rotating case $f = 0$, there is no low-frequency drop-off in h_0 as $\omega \rightarrow 0$.

These properties of h_0 can be used to write down an approximate expression for D in the admittedly artificial case where the wave spectrum is localized in some narrow wavenumber and frequency range ΔK and $\Delta\omega$ centred around some fixed K and ω . It then follows from (5.11), (5.15) and (2.18)–(2.19) that

$$\begin{aligned} D &= \frac{1}{4} \frac{1}{(2\pi)^3} \int_{\omega > 0} S(K_1, \omega) S(K_2, \omega) H_0(K_1, K_2, \omega) dK_1 dK_2 d\omega \\ &\approx \frac{2\pi}{4} \frac{K^2}{N^2} \frac{\bar{E}^2}{\Delta\omega} h_0(1, s, a) \approx 0.17 \frac{2\pi}{4} \frac{K^2}{N^2} \frac{\bar{E}^2}{\Delta\omega} \approx \frac{1}{4} \frac{K^2}{N^2} \frac{\bar{E}^2}{\Delta\omega}. \end{aligned} \quad (5.17)$$

The diffusivity diverges as the frequency bandwidth $\Delta\omega \rightarrow 0$ because the autocorrelation time diverges in this limit. The sensitivity of D to small-scale waves indicated by the factor K^2 is actually a general feature of arbitrary spectra; this is described in §6.2. A variant of the approximation (5.17) is applied to the standard ocean wave spectrum in §8.1.

6. Scaling properties and comparison with shallow-water dynamics

We now consider how D is affected by changes in the wave power spectrum whilst keeping the total wave energy constant. The spectral density $S(K, \omega)$ suggests two such basic changes by shifting the power spectrum either in total wavenumber K or in frequency ω . General frequency shifts do not lead to a simple scaling relation, but in §6.1 we explore shifts to very low frequencies near f by a combination of asymptotic expansion and numerics. Shifts in wavenumber K , on the other hand, do lead to a simple exact scaling relation listed in §6.2. We also compare these result to the shallow-water case studied in BHC; we use superscripts *SW* and *BQ* to distinguish between the two cases.

6.1. Frequency scaling

Suppose we start with a particular spectrum in the shallow-water or Boussinesq systems, $S^{SW}(\omega)$ or $S^{BQ}(K, \omega)$, with corresponding diffusivities D^{SW} , D^{BQ} . Let us use these to define a self-similar family of spectra by stretching the non-dimensional

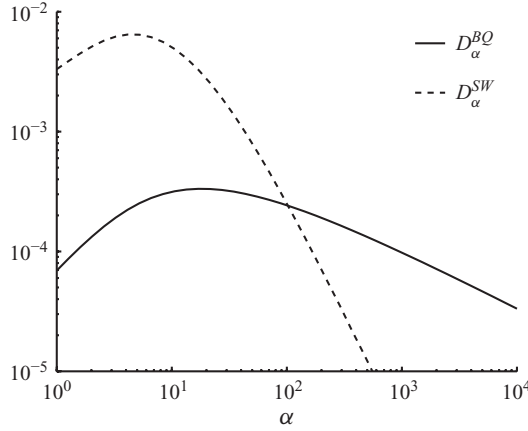


FIGURE 3. Diffusivity as a function of α for the spectra $S_\alpha^{SW}(s) = \alpha S^{SW}(\alpha s)$, $S_\alpha^{BQ}(K, s) = \alpha S^{BQ}(K, \alpha s)$, where the initial spectra are $S^{BQ}(K, \omega) = 1_{(0.1 \leq K \leq 4)} 1_{(2f \leq \omega \leq 3f)}$, $S^{SW}(\omega) = (1/2\pi) \int S^{BQ}(K, \omega) dK$. The shallow-water diffusivity approaches the power law $D_\alpha^{SW} \propto \alpha^{-2}$ for large α , while the Boussinesq diffusivity decreases much more slowly as $D_\alpha^{BQ} \propto \alpha^{-1/2}$. This means that the Boussinesq diffusivity is much less sensitive than the shallow-water diffusivity to the structure of the energy near f .

frequency s in (5.12) with a factor $\alpha > 0$, but keeping the energy constant:

$$S_\alpha^{SW}(s) = \alpha S^{SW}(\alpha s), \quad S_\alpha^{BQ}(K, s) = \alpha S^{BQ}(K, \alpha s). \quad (6.1)$$

In the above we have written the spectra in the s -space for convenience. (Note that in defining s for the shallow-water system we can use any value for N provided it is larger than f ; the results are independent of the particular number we choose.) We would like to know how the corresponding diffusivities D_α^{SW} , D_α^{BQ} depend on α in the limit $\alpha \rightarrow \infty$, i.e. as the energy moves closer and closer to f .

There is no exact scaling but by Taylor-expanding the relevant densities for small $s \ll 1$, we derived the asymptotic scalings

$$D_\alpha^{SW} = O(\alpha^{-2}), \quad D_\alpha^{BQ} = O(\alpha^{-1/2}), \quad (\alpha \rightarrow \infty). \quad (6.2)$$

The Boussinesq diffusivity shows a much weaker drop-off than the shallow-water diffusivity as the energy approaches the inertial frequency. This means that the Boussinesq diffusivity will be fairly insensitive to the precise structure of the energy near f , while the shallow-water diffusivity could drop several orders of magnitude with a small change in the energy near f . This scaling law is confirmed in the numerical calculations shown in figure 3, where D_α^{BQ} and D_α^{SW} are calculated exactly over a range of α for a particular initial spectrum. Notably, both diffusivities actually *increase* with α for moderate values of α before settling into the asymptotic decline for $\alpha \gg 1$. Presumably, this is because the effect of the spectrum getting narrower (and therefore reducing frequency bandwidth) with increasing α dominates the decrease in the diffusivity density at moderate α values, at least for the model spectrum chosen.

6.2. Wavenumber scaling

We can perform the same scaling in wavenumber space. Again, let us start with spectra $S^{SW}(\kappa)$ and $S^{BQ}(K, \omega)$, with corresponding diffusivities D^{SW} , D^{BQ} , and stretch these in wavenumber space while keeping the energy constant:

$$S_\alpha^{SW}(\kappa) = \alpha S^{SW}(\alpha \kappa), \quad S_\alpha^{BQ}(K, \omega) = \alpha S^{BQ}(\alpha K, \omega). \quad (6.3)$$

Here κ is the horizontal wavenumber magnitude in the shallow-water system. For the Boussinesq system, we easily obtain

$$\begin{aligned}
 D_\alpha^{BQ} &= \frac{1}{4} \frac{1}{(2\pi)^3} \int S_\alpha^{BQ}(K_1, \omega) S_\alpha^{BQ}(K_2, \omega) H_0(K_1, K_2, \omega) dK_1 dK_2 d\omega \\
 &= \frac{1}{4} \frac{1}{(2\pi)^3} \int S^{BQ}(\alpha K_1, \omega) S^{BQ}(\alpha K_2, \omega) H_0(K_1, K_2, \omega) d(\alpha K_1) d(\alpha K_2) d\omega \\
 &= \frac{1}{4} \frac{1}{(2\pi)^3} \int S^{BQ}(\bar{K}_1, \omega) S^{BQ}(\bar{K}_2, \omega) \frac{1}{\alpha^2} H_0(\bar{K}_1, \bar{K}_2, \omega) d\bar{K}_1 d\bar{K}_2 d\omega = \frac{1}{\alpha^2} D^{BQ}.
 \end{aligned} \tag{6.4}$$

This exact result, which is consistent with the special case (5.17), uses the second-order homogeneity of H_0 in (5.14) and the substitution $\bar{K}_i = \alpha K_i$. A similar exact result in shallow-water theory is available only in the non-rotating case, hence we obtain

$$f = 0 : \quad D_\alpha^{SW} = \alpha D^{SW}, \quad \text{and} \quad f \geq 0 : \quad D_\alpha^{BQ} = \frac{1}{\alpha^2} D^{BQ}. \tag{6.5}$$

The two systems show contrasting scaling properties: in the non-rotating shallow-water system, the diffusivity increases as energy goes to *larger* scales ($\alpha > 1$), but in the Boussinesq system the diffusivity increases as energy goes to *smaller* scales ($\alpha < 1$). As far as the Boussinesq system is concerned, the main point to take away from (6.5) is that the diffusivity density for a given wave frequency is sensitive to small-scale waves.

7. Monte-Carlo simulations

We performed Monte-Carlo simulations as an independent check on the algebra involved in deriving the diffusivity density in (5.11). We used a discretized version of (2.9) (see BHC for details) to generate samples of wave field, from which we calculated the Lagrangian velocity by solving (3.10) for the streamfunction. The time-correlation function was then calculated as an average of the time correlations over every point in the domain and all samples.

The spectra were chosen to be narrow in the ω -space and the location of the central frequency varied so as to highlight the frequency-dependence of the diffusivity; with arbitrary length and time scales, they were of the form

$$S(K, \omega) = \frac{(2\pi)^2 \bar{E}}{\Delta K \Delta \omega} 1_{(0.45 \leq K \leq 0.75)} 1_{(\omega_0 \leq \omega \leq \omega_0 + \Delta \omega)}, \tag{7.1}$$

where $\Delta \omega = (N - f)\Delta s$, $\Delta s = 0.15$, $\omega_0 = (N - f)s_0 + f$, and s_0 varied from 0 to 0.8. The other parameters were $\bar{E} = 0.25$, $\Delta K = 0.3$, $N = 5$, $f = 1$, so the Prandtl ratio was $a = 0.2$. The parameters for the discretization were chosen such that the lengths of the domains were $L_x = L_y = 200$, $L_z = 100$, the numbers of points in each direction were $N_x = N_y = 2^7$, $N_z = 2^6$. The samples were generated for 40 units of time at intervals of 0.625, and the diffusivity was calculated by summing the correlation functions up to 10 units of time. (This was the time after which the correlations had approximately decayed to zero; beyond this all that remained were random numbers and a mean component induced by the discretization.) The discretized spectra were multiplied by a factor, different for each spectrum, to make the expected energy in the discretized versions of the spectra equal to that of the continuous spectrum, \bar{E} . The results are shown in figure 4. The Monte-Carlo diffusivities agree closely with

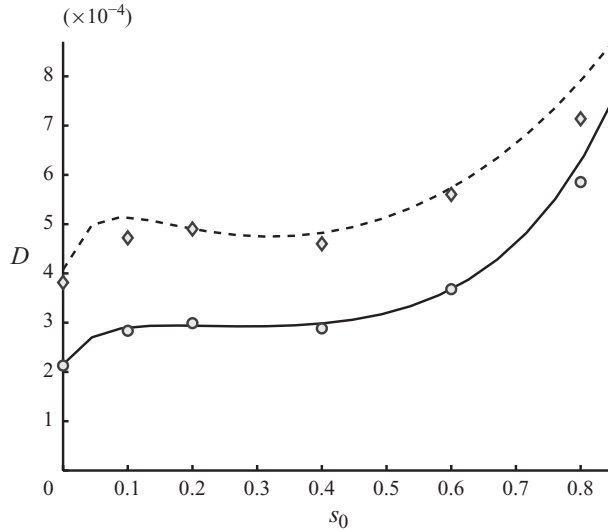


FIGURE 4. Theoretical diffusivity (lines) and diffusivity computed from the Monte-Carlo simulations (markers), as a function of the most energetic non-dimensional frequency s_0 (see text for exact form of spectrum as a function of s_0). The dashed lines/diamonds correspond to spectra where the waves travel in the same vertical direction, while the solid lines/circles have equal energy in waves of both directions.

the theoretical results obtained by integrating (5.11). Most of the error is due to the spatial discretization of the power spectrum, as it was expensive to represent a narrow-banded frequency spectrum in three spatial dimensions; there is very little statistical error. Thus, we are confident that our formula (5.11) is correct.

8. Oceanic applications

A practical motivation of the present work was to study the dispersion of tracers induced by internal waves in the ocean. Studies of tracer dispersion in the ocean have focused mainly on the effect of vortical flows, i.e. flows characterized by the coherent structures that emerge as a consequence of conservation laws associated with non-uniform potential vorticity. These motions dominate tracer transports at horizontal scales much larger than the ocean depth. However, in addition to vortical motions, the ocean is filled with an energetic internal wave field. Internal waves are ubiquitous and show up everywhere in temperature, salinity and velocity measurements at horizontal scales below 10 km and frequencies above f (e.g. Munk 1981). In this section, we apply our results on tracer dispersion to the oceanic internal wave field. The goal is to assess how efficient are oceanic internal waves at dispersing tracers at horizontal scales below 10 km. The results will be contrasted with dispersion by other mechanisms.

8.1. Dispersion by the Garrett–Munk internal wave spectrum

The internal wave field in the ocean consists of a superposition of many waves with different frequencies, wavenumbers and amplitudes. Waves are generated by various processes such as surface winds, tidal and geostrophic flows impinging over topography. Once generated they radiate and fill the ocean interior, undergoing nonlinear interactions in the process, before they break and dissipate. The result is a fairly random and ubiquitous wave continuum best described statistically in terms

of a wavenumber–frequency spectrum. Observations (e.g. Levine *et al.* 1997) suggest that in the deep ocean, away from surface and bottom boundary layers, the spectrum can be divided into three separate components: (i) near-inertial waves that have frequencies close to the local inertial frequency, (ii) tides at both the semidiurnal and diurnal frequencies and (iii) the internal wave *continuum* between frequencies f and N . Near-inertial waves are generated principally in the upper ocean by storms and propagate in the interior, and therefore exhibit considerable variability in time and space. Tides are also site-specific and depend on the basin shape and the bottom topography. Only the continuum is remarkably steady in time and homogeneous in space, and hence describable by a universal spectrum (Munk 1981). Consequently, we will first focus our attention to the dispersion induced by the continuum component, because the results will be relevant for most of the ocean interior. We will then comment on the role of near-inertial waves and tides on the lateral dispersion of tracers in a specific area of the ocean, where the data necessary for the calculation are available.

The Garrett–Munk (1981) model spectrum provides an analytical representation of energy in the wave continuum. The model was derived by fitting measurements from many locations and different depths, and it reproduces quite accurately the shape and the energy level of the internal wave continuum. The standard form of the model spectrum, known as GM81, is given in the (ω, j) -space, where j is the vertical mode number. We will work with the continuous form of the spectrum given in the (ω, m) -space on the positive quadrant by using the Wentzel–Kramers–Brillouin approximation:

$$S^{GM}(m, \omega) = (2\pi)^2 \bar{E} \left(\frac{2}{\pi} \frac{m_*}{m_*^2 + m^2} 1_{|m| < m_c} \right) \left(\frac{2}{\pi} \frac{f}{\omega \sqrt{\omega^2 - f^2}} 1_{f \leq \omega \leq N} \right), \quad (8.1)$$

where

$$\bar{E} = E_0 b^2 N_0 N, \quad m_* = \frac{3\pi}{b} \frac{N}{N_0}, \quad m_c = \frac{2\pi}{10 \text{ m}}, \quad (8.2)$$

$$E_0 = 6.3 \times 10^{-5}, \quad b = 1300 \text{ m}, \quad N_0 = 5.2 \times 10^{-3} \text{ s}^{-1}. \quad (8.3)$$

This WKB approximation allows for deviations of the local buoyancy frequency N from the reference value N_0 , in which case both the local energy density \bar{E} and the local central wavenumber m_* are taken as proportional to N .

The GM81 spectrum is converted into (K, ω) -space by first substituting the internal wave dispersion relationship $m^2 = ((N^2 - f^2)/(N^2 - \omega^2))K^2$ wherever m^2 appears in (8.1) and then multiplying by the Jacobian of the transformation $\partial K / \partial m = \sqrt{(N^2 - f^2)/(N^2 - \omega^2)}$. The resulting diffusivity is unbounded, because the GM81 spectrum has finite energy at $\omega = N$, where the Jacobian of the transformation has a non-integrable singularity. In practice, this is not a serious issue, because there is little energy near the buoyancy frequency and it is physically reasonable to truncate the spectrum near $\omega = N$. We choose a simple form of the truncation by replacing the cutoff in the m -space, $1_{|m| < m_c}$, with a cutoff in the K -space, $1_{K < m_c}$. Because there is very little energy in the spectrum when ω is far away from f , the estimates presented below are insensitive to any reasonable form of truncation.

We can now calculate the diffusivity D by substituting the GM81 spectrum into (5.9) and setting $N = 4.0 \times 10^{-3} \text{ s}^{-1}$ and $f = 10^{-4} \text{ s}^{-1}$ (we use the same values as chosen by Young, Rhines & Garrett (1982) in their study of shear dispersion to help in the comparison between our and their results). The integral is evaluated numerically

using a Monte-Carlo integration with 2^{23} points. We obtain

$$\text{GM81}(N = 4 \times 10^{-3} \text{ s}^{-1}, f = 1 \times 10^{-4} \text{ s}^{-1}) : \quad D = 0.01 \text{ m}^2 \text{ s}^{-1} \quad (8.4)$$

with negligible numerical error. The actual number should not be taken too literally, because the integral for D is affected significantly by wave frequencies between f and $2f$ because these contain the bulk of the energy in the GM81 spectrum. In the real ocean, near-inertial waves, which are variable in space and time, dominate the energy content in this frequency band, but they are not captured by the universal GM81 form. Since wave-induced dispersion is proportional to the square of the energy in a given frequency band, the associated D can change by orders of magnitude with the uncertainty in the inertial peak.

Interestingly, (8.4) is close (a factor of three smaller) to the GM81 diffusivity estimate computed in §3.3 of Davis (1991) using a particular turbulence closure. However, in that estimation, the diffusivity was proportional to the wave energy rather than the wave energy squared, as is the case here. Therefore, the closeness of the numerical values is probably coincidental.

We can compare (8.1) with a scaling estimate based on the pseudomomentum of the wave field, following the line of argument described in §4, in which the Lagrangian-mean flow is approximated by the pseudomomentum. This estimate does produce the correct proportionality $D \propto \bar{E}^2$, but the coefficient is much too large for the reasons described in §4. For example, if we take $1/f$ as the autocorrelation time of the GM81 wave field and multiply this by the square of the expected value of the horizontal pseudomomentum magnitude for plane waves

$$\left(\frac{1}{(2\pi)^2} \int \frac{\kappa}{\omega} S^{GM} \, d\mathbf{m} \, d\omega \right)^2 \approx 2 \times 10^{-5} \text{ m}^2 \text{ s}^{-2}, \quad (8.5)$$

then we obtain an estimated diffusivity of $D \approx 0.2 \text{ m}^2 \text{ s}^{-1}$. This is much larger than the true value of $0.01 \text{ m}^2 \text{ s}^{-1}$ computed above.

8.2. Dependence on the parameters of the GM81 spectrum

We can discern the dependence of D on the parameters of the GM81 spectrum by using an approximate expression for the diffusivity based on the analysis in §5.3 and the approximation $m \approx K$, which is valid for low-frequency internal waves. Details are given in §A.3, and the result is

$$D \approx 0.08 \frac{\bar{E}^2 m_*^2}{N^2 f} \left\{ 2 \ln \left(\frac{m_c}{m_*} \right) - \frac{\pi^2}{4} \right\}, \quad (8.6)$$

which delivers $0.05 \text{ m}^2 \text{ s}^{-1}$ instead of $0.01 \text{ m}^2 \text{ s}^{-1}$ in (8.4). Clearly, the pre-factor in (8.6) is quite inaccurate, but we have checked that this formula does give the correct scaling of D with the parameters of GM81. Specifically, this expression corroborates the weak dependence of D on m_c and it also highlights the proportionality of D to $\bar{E}^2 m_*^2$. Interestingly, there is an inverse proportionality of D on the Coriolis parameter f , which indicates an increase of D towards the equator. Finally, in order to judge the dependence of D on N , one needs to include the linear dependence of both \bar{E} and m_* on N that is part of the definition of the GM81 spectrum in (8.1). This yields the overall scaling $D \propto (\bar{E} m_*)^2 / N^2 \propto N^2$, so diffusion due to the GM81 spectrum can be expected to *increase* with stronger stratification.

8.3. Comparison of wave-induced dispersion and shear dispersion

It is useful to compare our value for D with the value obtained by Young *et al.* (1982) for internal wave shear dispersion. Young and collaborators showed that internal wave shear, combined with vertical mixing by wave breaking, generates lateral dispersion of tracers. Using their formula and the form of the GM spectrum in (8.1), one obtains

$$D^Y \approx \kappa_t \frac{\bar{E} m_* m_c}{\pi f^2} \left[1 + \frac{1}{2} \log \left(\frac{f}{m_c^2 \kappa_t} \right) \right], \quad (8.7)$$

where κ_t is the turbulent vertical diffusivity generated by wave breaking. The logarithmic correction stems from a decaying power-law tail added to the GM spectrum for $m > m_c$, as is sometimes done in the oceanographic literature. Notably, D^Y is proportional to \bar{E} , not \bar{E}^2 .

Using the same parameters as reported above and $\kappa_t = 1.0 \times 10^{-5} \text{ m}^2 \text{ s}^{-1}$, we estimate $D^Y \approx 0.007 \text{ m}^2 \text{ s}^{-1}$. (This value is about half the value reported by Young *et al.* 1982, because the shear in GM81 is about half the value used by Young and collaborators.) This is about half of the value in (8.1), so we believe that in typical ocean situations, wave-induced dispersion could be of equal or greater magnitude than shear dispersion.

A comparison of formulae (8.6) and (8.7) highlights major differences between the two processes. Wave-induced dispersion is quadratic in \bar{E} , and hence most effective in regions with a strong internal wave field. Shear dispersion instead is largest when waves are vigorously breaking and κ_t is large.

Last but not least, a caveat should be added here regarding the vertical cutoff wavenumber m_c in (8.6). The wave-induced diffusivity is not sensitive to the choice of m_c , but the shear dispersion increases noticeably with the cutoff wavenumber m_c . Shear dispersion is dominated by waves with small vertical scales of orders of a few metres, while wave-induced dispersion is primarily the result of deep waves with vertical scales of a few hundred metres. Hence, the two processes are likely to act in parallel with shear dispersion dominating at small scales and wave-induced dispersion taking over at horizontal scales larger than $O(1) \text{ km}$.

8.4. Dispersion by internal waves during NATRE

A more quantitative estimate of internal wave-induced dispersion can be done using internal wave data from a specific location. We focus on the eastern subtropical North Atlantic which was the subject of an intensive series of field programmes in 1991–1993 as part of the NATRE (Ledwell, Watson & Law 1998), and the subduction experiment (Joyce *et al.* 1998).

A moored array was deployed as part of the subduction experiment (Weller *et al.* 2004) at 25.5N and 29W. The array was equipped with vector-averaging current meters at depths of 200, 300, 310, 1500 and 3500 m and recorded velocity for two years (summer 1991–spring 1993). The frequency spectrum from the 300 m current meter is shown in figure 5. For comparison, the dashed line shows the GM81 spectrum. There are clear differences between the two spectra, in particular at low frequencies, where the GM81 spectrum does not capture the tidal and inertial peaks.

A high-resolution profiler (HRP) was used as part of NATRE and provides vertical profiles of velocity for the same region as the current-meter data (Polzin & Ferrari 2004). Polzin, Toole & Schmitt (1995) reported that the spectrum of the horizontal velocity rolls off as m^{-2} , consistent with the GM81 model. If we repeat the GM81 computation using the local NATRE values $N = 4.3 \times 10^{-3} \text{ s}^{-1}$ and f according to

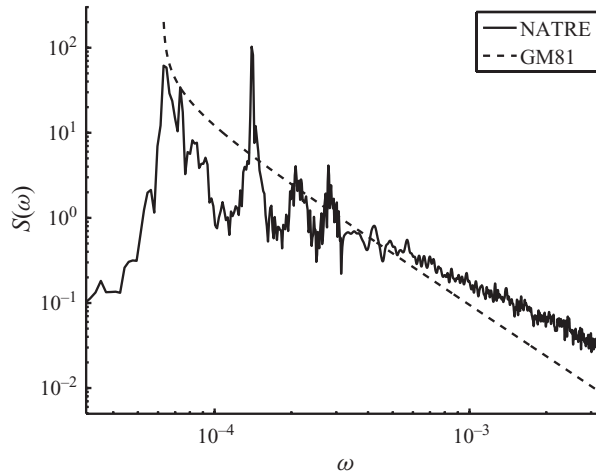


FIGURE 5. Marginal frequency spectra for the GM81 spectrum (dashed line), obtained by integrating (8.1) over m , and for mooring data collected as part of NATRE (solid line).

25° latitude, we obtain

$$\text{GM81}(N = 4.3 \times 10^{-3} \text{ s}^{-1}, \quad f = 6.15 \times 10^{-5} \text{ s}^{-1}) : \quad D = 0.02 \text{ m}^2 \text{ s}^{-1}, \quad (8.8)$$

which is about twice the value in (8.4), consistent with the increase in N^2/f .

We also constructed a provisional model spectrum for the region by replacing the frequency dependence of the GM81 model spectrum in (8.1) with the frequency spectrum measured by the current meter displayed in figure 5. This was used to compute the diffusivity at 300 m and returned the larger value of

$$\text{measured frequency spectrum} : \quad D = 0.04 \text{ m}^2 \text{ s}^{-1}. \quad (8.9)$$

The measured frequency spectrum has less energy in the inertial range, but more than compensates for this by the narrow-banded energy in the tidal peaks. Indeed, we estimate that these tidal peaks contribute more than 90 % of the total in (8.9). The tidal peaks dominate the dispersion because we have shown that narrow spectra generate larger diffusivities than broad ones (cf. $\Delta\omega$ in the denominator of (5.17)), and because they have frequencies farther away from f .

As described by Ledwell, Watson & Law (1993) and Ledwellet *al.* (1998), a passive tracer was released at 300 m depth during the NATRE experiment. Following the spreading of tracer filaments for a couple of weeks, they inferred a lateral diffusivity $O(1) \text{ m}^2 \text{ s}^{-1}$ on horizontal scales of 1–10 km. This diffusivity is much larger than the molecular value of the order of $10^{-9} \text{ m}^2 \text{ s}^{-1}$, so larger-scale processes must be responsible for the spreading. Internal wave-induced dispersion appears to be an order of magnitude too small to match observations. Dispersion by vortical flows, such as those generated by wave-breaking events (Polzin & Ferrari 2004) or by filamentation from mesoscale stirring (Smith & Ferrari 2009), appears to be more likely candidates to explain observations in NATRE.

9. Concluding comments

We have put together a theory and a computational tool for the evaluation of the one-particle horizontal diffusivity D due to small-amplitude Gaussian random

internal waves in the rotating Boussinesq system. The main formula which will be useful for numerical calculations is (5.9), where integration kernels $G_1(K_1, K_2, \omega, \theta)$, $G_2(K_1, K_2, \omega, \theta)$ are given in the Appendix (§A.2) and $S_{up}(K_1, \omega)$, $S_{down}(K_2, \omega)$ are horizontally isotropic wave power spectra for waves going vertically upwards and downwards (see (2.18) and (2.19) for correct normalizations). We found it most efficient to evaluate the formula using a numerical Monte-Carlo integration.

We found in §§5 and 6 that the one-particle horizontal diffusivity is suppressed by rotation and is most sensitive to small-scale waves (in contrast to shallow-water waves, which disperse most effectively at large scales). In §6, we also showed that the incompressibility constraint for the second-order Lagrangian velocity strongly limits the wave interactions that contribute to dispersion and makes a three-dimensional wave field less dispersive than an equivalently energetic shallow-water wave field. Finally, in §8 we applied our theory to the oceanic setting by computing how much the background internal wave field, as described by both the Garrett–Munk spectrum and detailed field observations from the NATRE, might contribute to horizontal dispersion of tracers at horizontal scales less than 10 km. We compared this mechanism with another known mechanism of diffusion by a wave field, namely shear dispersion, and find the former to be comparable or greater in magnitude for typical ocean wave spectra, although the two possess qualitatively different features and are preferred under different conditions.

The one-particle diffusivity, as discussed in §1, is of course not sufficient to determine the general dispersion characteristics of tracer fields, which in principle would require two-particle diffusivities or even higher-order diffusivities. Still, for sufficiently well-separated particles, these higher-order diffusivities can be related to D , e.g. the two-particle diffusivity asymptotes to $2D$ for large particle separations if the wave field has a finite horizontal correlation scale. This was demonstrated for shallow-water waves in detail in BHC, where the full two-particle diffusivity tensor was computed numerically. We hence presume that for naturally occurring wave fields, D is a good estimate for the wave-induced tracer diffusivity due to Gaussian random waves.

A much more subtle question concerns the importance of the Gaussian assumption. We made this assumption because of its simplicity and because it leads to an unambiguous expression for D as a functional of the wave power spectrum. However, many different wave fields can give rise to the same power spectrum and there is no guarantee that they would give rise to the same diffusivities. We think that it would be of fundamental interest to investigate the sensitivity of D to the Gaussian assumption.

For instance, in another modelling extreme, one could allow the wave field realizations to consist of a random superposition of wavepackets. This would lead to a situation much closer to the slowly varying wavetrain set-ups studied in BM and Bühler (2009). Such a wavepacket scenario does not contradict the assumption of a spatially homogeneous zero-mean wave field, because the latter assumption is satisfied precisely if all Fourier coefficients are uncorrelated, but only under the additional assumption of a Gaussian wave field does this imply that the Fourier coefficients are statistically independent.

In oceanography, the assumption of Gaussian waves is sometimes justified by the physical fact that at a given location, one finds a superposition of waves that have propagated long distances from many different sources, thus effectively randomizing the phase of the wave field. Still, the generic result of long-distance propagation in a dispersive wave system is a slowly varying wavetrain, not a Gaussian random wave field, so it appears natural to investigate the diffusion based on such wavetrains

or wavepackets. At any rate, present observations cannot distinguish between these alternative interpretations of the wave power spectra.

Interestingly, in the heuristic analysis presented in §4 the assumption of random wavepackets would lead to an entirely different set of wave-wave interaction terms becoming important for the Lagrangian flow. In fact, if the results of BM were to turn out to be generic, then it would appear that the approximation $\mathbf{u}^L \stackrel{!}{=} 0.5\mathbf{p}$ in the incompressibility constraint might lead to basically the correct value for D . Apparently, this would mean that for the same level of wave energy, random wavepackets are more efficient at diffusing particles than Gaussian random waves, at least in three-dimensional flows. Conversely, for shallow-water waves, we would expect little or no difference between the two cases. This is a subject for further research.

S. Yang performed and analysed some numerical simulations of particle trajectories as part of an undergraduate research experience at New York University. Financial support for O.B. under the United States National Science Foundation grant DMS-0604519 is gratefully acknowledged. M.H.C. is supported in part by a Canadian NSERC PGS-D scholarship. R.F. acknowledges support through ONR grant N000140910458.

Appendix

A.1. Derivation of (5.9)

We summarize how to derive (5.9) in the special case where there are only upward-propagating waves. Substitution from (2.16) into (5.7) produces the non-zero δ -function combinations

$$\delta(\omega_1 - \omega(\beta_1))\delta(\omega_1 - \omega(\beta_2)) + \delta(\omega_1 + \omega(\beta_1))\delta(\omega_1 + \omega(\beta_2)) \quad (\text{A } 1)$$

multiplied by the group velocity indicator functions

$$1_{\text{sgn}(\beta_1)=\text{sgn}(\omega_1)}1_{\text{sgn}(\beta_2)=-\text{sgn}(\omega_1)}. \quad (\text{A } 2)$$

Integration over ω_1 then yields $\delta(\omega(\beta_1) - \omega(\beta_2))$ times two instances of the function g evaluated at different arguments. Integration over β_2 then removes this δ -function and enforces $\beta_2 = \pm |\beta_1|$ in the remaining integral, which can be rewritten as an integral over $\beta_1 > 0$ and then converted into an integral over $\omega > 0$ such that $\beta_1 = \beta(\omega)$. Using the transformation rule (2.19) for the energy density then gives (5.9).

The terms for other wave direction combinations can be computed analogously and the simple expressions in (5.10) then follow after making use of two discrete symmetries of the function g in (5.8), namely that g remains unchanged if the signs of *both* its β arguments are flipped, or if the signs of *both* its ω arguments are flipped. These symmetries of g can be traced back to the symmetries of the linear equations of motion under a reversal of the vertical coordinate or the time coordinate.

A.2. Explicit expressions

Theses quantities appear in §5. The arguments of all the trigonometric functions are single angles only, e.g. in a term $\sin \beta_2 \omega_1$ the factor ω_1 multiplies $\sin \beta_2$, and

so on:

$$\begin{aligned} \gamma(\mathbf{K}_1, \mathbf{K}_2) = & \frac{N^2 K_1 K_2}{2\omega_1^2 \omega_2^2} (-f(-\cos \beta_1 \sin \beta_2 \omega_1 \\ & + \cos \beta_2 \sin \beta_1 \omega_1 \cos \theta - i f \cos \beta_2 \sin \beta_1 \sin \theta) \\ & \times (-\cos \beta_2 \sin \beta_1 \omega_2 + \cos \beta_1 \sin \beta_2 \omega_2 \cos \theta + i f \cos \beta_1 \sin \beta_2 \sin \theta) \\ & + \cos \beta_1 \cos \beta_2 \sin \theta (-2i \cos \beta_1 \cos \beta_2 \omega_1 \omega_2^2 + i \sin \beta_1 \sin \beta_2 (-2\omega_1 \omega_2^2 \\ & + f^2(\omega_1 + \omega_2)) \cos \theta + f \sin \beta_1 \sin \beta_2 (f^2 + (\omega_1 - 2\omega_2)\omega_2) \sin \theta)), \quad (\text{A } 3) \end{aligned}$$

$$\begin{aligned} G_1(K_1, K_2, \omega, \theta) = & \frac{N^4 \cos^4 \beta K_1^2 K_2^2}{\omega^6} (4f^2 \omega^2 \sin^4 \beta (1 + 2 \cos \theta)^2 \sin^4 \theta / 2 \\ & + (-f^2 \sin^2 \beta + \omega^2 \cos^2 \beta + (f^2 + \omega^2) \sin^2 \beta \cos \theta)^2 \sin^2 \theta) \\ & \times \frac{\cos^2 \beta (K_1^2 + K_2^2 + 2K_1 K_2 \cos \theta)}{(N^2 \cos^2 \beta (K_1^2 + K_2^2 + 2K_1 K_2 \cos \theta) + f^2 (K_1 + K_2)^2 \sin^2 \beta)^2}, \quad (\text{A } 4) \end{aligned}$$

$$\begin{aligned} G_2(K_1, K_2, \omega, \theta) = & \frac{N^4 \cos^4 \beta K_1^2 K_2^2}{\omega^6} (4f^2 \omega^2 \sin^4 \beta (1 - 2 \cos \theta)^2 \cos^4 \theta / 2 \\ & + (f^2 \sin^2 \beta - \omega^2 \cos^2 \beta + (f^2 + \omega^2) \sin^2 \beta \cos \theta)^2 \sin^2 \theta) \\ & \times \frac{\cos^2 \beta (K_1^2 + K_2^2 + 2K_1 K_2 \cos \theta)}{(N^2 \cos^2 \beta (K_1^2 + K_2^2 + 2K_1 K_2 \cos \theta) + f^2 (K_1 - K_2)^2 \sin^2 \beta)^2}, \quad (\text{A } 5) \end{aligned}$$

where

$$\cos^2 \beta = \frac{\omega^2 - f^2}{N^2 - f^2}, \quad \sin^2 \beta = \frac{N^2 - \omega^2}{N^2 - f^2}, \quad \theta = \theta_1 - \theta_2. \quad (\text{A } 6)$$

$$H_0|_{f=0}(K_1, K_2, \omega) = \frac{K_1^2}{8N^6 K_2^2} (K_1^2 (N^2 - \omega^2)^2 + K_2^2 (N^4 - 2N^2 \omega^2 + 5\omega^4)), \quad (K_1 \leq K_2). \quad (\text{A } 7)$$

$$\begin{aligned} H_1|_{f=0}(K_1, K_2, \omega) = & \frac{K_1^2}{8N^6 K_2^2} (K_1^2 (N^2 - \omega^2)^2 - 4K_1 K_2 \omega^2 (N^2 - \omega^2) \\ & + K_2^2 (N^4 - 2N^2 \omega^2 + 5\omega^4)), \quad (K_1 \leq K_2). \quad (\text{A } 8) \end{aligned}$$

$$\begin{aligned} H_2|_{f=0}(K_1, K_2, \omega) = & \frac{K_1^2}{8N^6 K_2^2} (K_1^2 (N^2 - \omega^2)^2 + 4K_1 K_2 \omega^2 (N^2 - \omega^2) \\ & + K_2^2 (N^4 - 2N^2 \omega^2 + 5\omega^4)), \quad (K_1 \leq K_2). \quad (\text{A } 9) \end{aligned}$$

In the last three expressions, the subscripts need to be switched if $K_2 \leq K_1$.

A.3. Derivation of approximate GM81 diffusivity

Using (5.12), (5.13), (5.15) and (5.16), the integral expression for the diffusivity (5.11) can be significantly simplified. After observing that the wavenumber integrals are symmetric, we can write the expression as twice an integral over $K_1 \geq K_2$ only, which

yields

$$D = \frac{1}{2} \frac{1}{(2\pi)^3} \frac{1}{N^2} \int_{\omega>0} \frac{\omega-f}{f} \left(\int S(K_1, \omega) dK_1 \int_0^{K_1} K_2^2 S(K_2, \omega) dK_2 \right) d\omega. \quad (\text{A } 10)$$

The main weakness of this approximation is that (5.16) overestimates the h_0 -function for larger $(\omega - f)/f$. For GM81, we obtain

$$D = \frac{1}{2} \frac{4^4}{(2\pi)^3} \frac{\bar{E}^2}{N^2} \int_f^N \frac{\omega-f}{f} \frac{f^2}{\omega^2(\omega^2 - f^2)} d\omega \int_0^{K_c} \frac{m_*}{m_*^2 + m_1^2} dK_1 \int_0^{K_1} K_2^2 \frac{m_*}{m_*^2 + m_2^2} dK_2. \quad (\text{A } 11)$$

For waves with frequency close to f (which contain most of the energy in the GM81 spectrum), $K \approx m$ and, therefore,

$$D = \frac{16}{\pi^3} \frac{\bar{E}^2}{N^2} \frac{m_*^2}{f} \int_1^{N/f=\infty} \frac{dx}{x^2(1+x)} \int_0^{m_c/m_*} \frac{d\mu_1}{1+\mu_1^2} \int_0^{\mu_1} \frac{\mu_2^2}{1+\mu_2^2} d\mu_2, \quad (\text{A } 12)$$

$$\approx \frac{16(1-\ln 2)}{\pi^3} \frac{\bar{E}^2}{N^2} \frac{m_*^2}{f} \int_0^{m_c/m_*} \frac{\mu_1 - \arctan(\mu_1)}{1+\mu_1^2} d\mu_1, \quad (\text{A } 13)$$

$$\approx 0.08 \frac{\bar{E}^2}{N^2} \frac{m_*^2}{f} \left(\log \left(1 + \left(\frac{m_c}{m_*} \right)^2 \right) - \left(\arctan \frac{m_c}{m_*} \right)^2 \right), \quad (\text{A } 14)$$

$$\approx 0.08 \frac{\bar{E}^2}{N^2} \frac{m_*^2}{f} \left(2 \log \left(\frac{m_c}{m_*} \right) - \frac{\pi^2}{4} \right). \quad (\text{A } 15)$$

We verified that this expression captures accurately the parametric dependence of D on \bar{E} , m_* , m_c , N and f . The prefactor 0.08 is instead too large. A more accurate expression can be obtained by splitting the integral in frequency and using the different approximations for h_0 at low frequencies and high frequencies given in (5.16). We do not pursue these embellishments, because we use (A 12) to discuss the dependence of D on the GM81 parameters.

REFERENCES

- ANDREWS, D. G. & MCINTYRE, M. E. 1978 An exact theory of nonlinear waves on a Lagrangian-mean flow. *J. Fluid Mech.* **89**, 609–646.
- BALK, A. M. 2006 Wave turbulent diffusion due to the Doppler shift. *J. Stat. Mech.* P08018.
- BALK, A. M., FALKOVICH, G. & STEPANOV, M. G. 2004 Growth of density inhomogeneities in a flow of wave turbulence. *Phys. Rev. Lett.* **92**, 244504.
- BALK, A. M. & McLAUGHLIN, R. M. 1999 Passive scalar in a random wave field: the weak turbulence approach. *Phys. Lett. A* **256**, 299–306.
- BATCHELOR, G. 1952 Diffusion in a field of homogeneous turbulence. ii. The relative motion of particles. *Proc. Camb. Phil. Soc.* **48**, 345–362.
- BÜHLER, O. 2009 *Waves and Mean Flows*. Cambridge University Press.
- BÜHLER, O. & HOLMES-CERFON, M. 2009 Particle dispersion by random waves in rotating shallow water. *J. Fluid Mech.* **638**, 5–26.
- BÜHLER, O. & MCINTYRE, M. E. 1998 On non-dissipative wave-mean interactions in the atmosphere or oceans. *J. Fluid Mech.* **354**, 301–343.
- CHERTKOV, M., FALKOVICH, G., KOLOKOLOV, I. & LEBEDEV, V. 1995 Statistics of a passive scalar advected by a large-scale two-dimensional velocity field: analytic solution. *Phys. Rev. E* **51** (6), 5609–5627.
- DAVIS, R. E. 1991 Observing the general circulation with floats. *Deep-Sea Res.* **28** (1), S531–S571.
- HERTERICH, K. & HASSELMANN, K. 1982 The horizontal diffusion of tracers by surface waves. *J. Phys. Oceanogr.* **12**, 704–712.

- LEDWELL, J., WATSON, A. & LAW, C. 1993 Evidence for slow mixing across the pycnocline from an open-ocean tracer-release experiment. *Nature* **364**, 701–703.
- LEDWELL, J., WATSON, A. & LAW, C. 1998 Mixing of a tracer in the pycnocline. *J. Geophys. Res.* **103** (C10), 21499–21529.
- JOYCE, T. M., LUYTEN, J. R., KUBRAYAKOV, A., BAHR, F. B. & PALLANT, J. 1998 Meso- to large-scale structure of subducting water in the subtropical gyre of the eastern North Atlantic Ocean. *J. Phys. Oceanogr.* **28**, 40–61.
- KRAICHNAN, R. H. 1970 Diffusion by a random velocity field. *Phys. Fluids* **13**, 22–32.
- LAMB, H. 1932 *Hydrodynamics*, 6th edn. Cambridge University Press.
- LEVINE, M. D., PADMAN, L., MUENCH, R. D. & MORISON, J. H. 1997 Internal waves and tides in the western Weddell Sea: observations from Ice Station Weddell. *J. Geophys. Res.* **102**, 1073–1090.
- LIGHTHILL, J. 1978 *Waves in Fluids*. Cambridge University Press.
- MAJDA, A. J. & KRAMER, P. R. 1999 Simplified models for turbulent diffusion: theory, numerical modelling, and physical phenomena. *Phys. Rep.* **314**, 237–574.
- MUNK, W. 1981 Internal waves and small-scale processes. In *Evolution of Physical Oceanography* (ed. B. Warren & C. Wunsch), pp. 264–291. MIT Press.
- POLZIN, K. & FERRARI, R. 2004 Isopycnal dispersion in NATRE. *J. Phys. Oceanogr.* **34**, 247–257.
- POLZIN, K. L., TOOLE, J. M. & SCHMITT, R. W. 1995 Finescale parameterizations of turbulent dissipation. *J. Phys. Oceanogr.* **25**, 306–328.
- SANDERSON, B. G. & OKUBO, A. 1988 Diffusion by internal waves. *J. Geophys. Res.* **93**, 3570–3582.
- SAWFORD, B. 2001 Turbulent relative dispersion. *Annu. Rev. Fluid Mech.* **33**, 289–317.
- SMITH, K. S. & FERRARI, R. 2009 The production and dissipation of compensated thermohaline variance by mesoscale stirring. *J. Phys. Oceanogr.* **39**, 2477–2501.
- TAYLOR, G. I. 1921 Diffusion by continuous movements. *Proc. Lond. Math. Soc.* **20**, 196–212.
- TOSCHI, F. & BODENSCHATZ, E. 2009 Lagrangian properties of particles in turbulence. *Annu. Rev. Fluid. Mech.* **41**, 375–404.
- VUCELJA, M., FALKOVICH, G. & FOUXON, I. 2007 Clustering of matter in waves and currents. *Phys. Rev. E* **75**, 065301.
- WEICHMAN, P. & GLAZMAN, R. 2000 Passive scalar transport by travelling wave fields. *J. Fluid Mech.* **420**, 147–200.
- WELLER, R. A., FUREY, P. W., SPALL, M. A. & DAVIS, R. E. 2004 The large-scale context for oceanic subduction in the Northeast Atlantic. *Deep-Sea Res. I* **51**, 665–699.
- YOUNG, W. R., RHINES, P. B. & GARRETT, C. J. 1982 Shear-flow dispersion, internal waves and horizontal mixing in the ocean. *J. Phys. Oceanogr.* **12**, 515–527.